Soft Matter

Journal Name

Depletion, melting and reentrant solidification in mixtures of soft and hard colloids

Daniela Marzi,[a] Barbara Capone,[a] John Marakis,[b,c] Maria Consiglia Merola,[b,d] Domenico Truzzolillo,[b,e] Luca Cipelletti,[e] Firmin Moingeon,[f] Mario Gauthier,[f] Dimitris Vlassopoulos,[b,c] Christos N. Likos,*[a] and Manuel Camargo*[g]

We present extensive experimental and theoretical investigations on the structure, phase behavior, dynamics and rheology of model soft-hard colloidal mixtures realized with large, multiarm star polymers as the soft component and smaller, compact stars as the hard one. The number and length of the arms in star polymers control their softness, whereas the size ratio, the overall density and the composition are additional parameters varied for the mixtures. A coarse-grained theoretical strategy is employed to predict the structure of the systems as well as their ergodicity properties on the basis of mode coupling theory, for comparison with rheological measurements on the samples. We discovered that dynamically arrested star-polymer solutions recover their ergodicity upon the addition of colloidal additives. At the same time the system displays demixing instability, and the binodal of the latter meets the glass line in a way that leads, upon addition of a sufficient amount of colloidal particles, to an arrested phase separation and reentrant solidification. We present evidence for a subsequent solid-to-solid transition well within the region of arrested phase separation, attributed to a hard-sphere-mixture type of glass, due to osmotic shrinkage of the stars at high colloidal particle concentrations. We systematically investigated the interplay of star functionality and size ratio with glass melting and demixing, and rationalized our findings by depletion of the big stars due to the smaller colloids. This new depletion potential in which, contrary to the classic colloid-polymer case, the hard component depletes the soft one, has unique and novel characteristics and allows the calculation of phase diagrams for such mixtures. This work covers a broad range of soft-hard colloidal mixture compositions in which the soft component exceeds the hard one in size and provides general guidelines for controlling the properties of such complex mixtures.

1 Introduction

Hard colloid-polymer mixtures have attracted the attention of the scientific community over the last two decades[1–4] due to their extremely interesting and complex phase behavior as a function of the polymer-to-colloid size ratio $q = 2R_g/\sigma_c$, where R_g is the average radius of gyration of the polymer, and σ_c is the colloid diameter. It is possible to distinguish two main limits as a function of the size ratio q: the $q < 1$ case is the so-called *colloidal limit* and

$q > 1$ is termed the *protein limit*. In the colloidal limit, the colloids are larger than the polymers and the main equilibrium properties of the system can be rationalized within the depletion picture, since the macromolecules act as depletants for the larger colloidal particles. In this case the Asakura and Oosawa approach (AO), in which the size ratio and polymer concentration can be used to tune the range and strength of the depletion interaction between the colloids, still remains the prototype and forms the guiding paradigm.[5,6] Besides the equilibrium phase diagram of the mixture, the AO model has allowed the theoretical description of a host of other features such as the presence of higher-order glass transitions, dynamic heterogeneities, and gel formation resulting from the attractive contribution to the colloid-colloid interaction potential.[7–10]

The protein limit is the case in which the radius of gyration of the polymers becomes larger than that of the colloid; the internal degrees of freedom of the macromolecules are no longer negligible and the overall polymer shape and its interaction with the colloid cannot be considered as spherical. Many body interactions start playing a crucial role, as every single macromolecule might interact with more than one colloidal particle. As a consequence of this added complexity, the polymer does not act exclusively as

[a] Faculty of Physics, University of Vienna, Boltzmanngasse 5, A-1090 Vienna, Austria.

[b] FORTH, Institute of Electronic Structure and Laser, Heraklion, Crete 70013, Greece.

[c] Department of Materials Science and Technology, University of Crete, Heraklion, Crete 71003, Greece.

[d] Dipartimento di Ingegneria Industriale e dell' Informazione, Seconda Università di Napoli, Via Roma 21, 81031 Aversa (Caserta), Italy.

[e] Laboratoire Charles Coulomb (L2C), UMR 5221 CNRS-Université de Montpellier, Montpellier, France.

[f] Department of Chemistry, University of Waterloo, Waterloo, Ontario N2L 3G1, Canada.

[g] Centro de Investigaciones en Ciencias Básicas y Aplicadas, Universidad Antonio Nariño - Campus Cali, Km 18 via Cali-Jamundí, 760030 Santiago de Cali, Colombia.

* Corresponding authors: christos.likos@univie.ac.at, manuel.camargo@uan.edu.co

† Electronic Supplementary Information (ESI) available: [DLS and rheology data]. See DOI: 10.1039/b000000x/

a simple depletant for the smaller colloidal particles and the relevant length scale for the depletion potential is defined by the polymer correlation length.[11–13]

Historically, colloid-polymer mixtures refer to a combination of hard colloids and linear polymers interacting via excluded volume repulsions. Such systems have been widely investigated for their rheological and dynamic properties, and for the variety of phase diagrams they present. In recent years, advances in experimental work as well as in theoretical and computational descriptions allowed the consideration of mixtures of star polymers and colloids. The former are branched polymer made of f chains anchored on a common core; such complex macromolecules were demonstrated to be highly versatile models for soft colloids. Depending on their functionality f, stars constitute entities intermediate between linear polymers ($f = 2$) and sterically stabilized (hard) colloids ($f \to \infty$). Binary mixtures of hard and soft colloids present a very rich phase space associated with a wide variety of dynamic responses.[14,15] The tunable softness of stars is responsible for the observation of anomalous structural behaviors for star polymer solutions, the formation of several crystal structures and of the re-entrant melting as the density of the system increases[16,17]. Moreover, for dense suspensions of high functionality stars ($f > 50$), a glass-like transition takes place, i.e., a dynamic arrest into an amorphous state featuring an extremely long relaxation time, which is further enhanced by polydispersity.[14,18]

Due to the complex dynamic picture arising from the study of solutions of star polymers, mixtures of such macromolecules are expected to offer greater versatility than their hard counterparts, both in terms of structural and rheological properties. Investigations of binary mixtures of star polymers with different functionalities and/or size ratios demonstrated the existence of multiple glassy states, ranging from repulsive glasses at low additive densities to attractive (re-entrant) ones for high additive concentrations.[19–22] Additionally, mixtures of large stars and small linear polymers present a rich phenomenology including osmotic shrinkage of the stars, phase separation (demixing), cluster formation, and melting of the glassy state upon addition of linear polymers.[23–28] Due to the soft nature of the small additives, the solution behaves similarly to traditional colloid-polymer mixtures in the colloidal limit and the polymers act as a depletant for the large soft-colloids.

For the mixtures mentioned above the small-sized additives are all soft and, in this sense, the systems are analogous to traditional colloid-polymer mixtures in the colloidal limit. On the other hand, when small, hard additives are incorporated in dense star polymer suspensions, the emerging properties are more akin to those of polymer-colloid mixtures in the protein limit, with the additional characteristic that the polymer component is not a semidilute mesh but rather a collection of distinct polymeric soft colloids. Moreover, such materials are related to nanocomposite polymeric materials consisting of hard nanoparticles dispersed in a soft polymeric matrix, and whose thermomechanical properties may be tailored by modifying the quality of the dispersion and/or the interfacial interactions.[29,30] Likewise, other closely related systems are (solvent-free) self-suspended hairy nanoparticles suspensions, recently introduced as unique materials allowing nearly ideal mixing of nanocomposites.[31,32]

The analysis of mixtures of star polymers and hard colloids in the limit of small stars has been the subject of investigations in the early 2000's,[33–35] whereas the opposite limit of large stars has been addressed in a very recent study.[36] It was shown that the addition of small, hard-like colloids to a star polymer glass leads to an arrested phase separation. By increasing the concentration of the small colloidal units, the previously glassified system melts; a further increase in the amount of colloidal component added leads to the appearance of a reentrant solid state, the latter being a consequence of the interplay between the structural arrest line of the repulsive glass and macroscopic demixing, i.e., an arrested phase separation (APS) due to the penetration of the glass line within the two-phase region delineated by the demixing binodal.[37–40] Experiments carried out on the aforementioned star-colloidal mixture for a specific star functionality, $f = 214$, and star-to-colloid size ratio, $q = 3$, yielded excellent quantitative parameter-free agreement when compared with theoretical predictions on the phase space and with the dynamic properties of the system. The theoretical study was carried out by employing a recently introduced coarse-grained description of the mixture.[41] In such a representation both star polymers (S) and hard colloids (H) are represented by spheres separated by a center-to-center distance r and interacting through effective potentials $V_{ij}(r)$ ($i, j = S, H$). The excellent agreement found in this approach and that will be pinpointed in the following sections of this paper, validates the extension of the theoretical analysis to different functionalities f and size ratios q.

The present work builds upon the previously reported results of Ref.[36], extending them to yet unexplored regions of the parameter space and thereby bringing forward novel results, insights and guidelines for the design of new soft composites with tunable flow properties. The purpose of this work is first to further elucidate the phenomena reported in Ref.[36] and, in particular, the interplay between structural arrest and phase separation between the two components. New experiments provide evidence for the phase separation and its location with respect to the dynamic arrest line. In addition, we explore the parameter space of star functionality and star-colloid size ratio to understand the Physics behind the structure of such mixtures and come up with design guidelines for such composite materials. Finally, we investigate the reentrant region and the solid-solid transitions present in the system, providing evidence and an interpretation for two distinct kinds of solids observed.

The rest of the paper is organized as follows: In Section 2, the theoretical approach and the experimental methods are presented. In Section 3, we focus our attention on the influence of small colloidal additives on melting of the glassy state of the stars, by exploring theoretically various combinations of functionalities and size ratios, and investigating experimentally the reentrance of solidification upon entering the phase separation region. Mode coupling theory calculations are compared with rheological linear viscoelastic measurements, and state diagrams are drawn displaying the estimated loci of both the liquid-glass and the demixing lines. In Section 4 we turn our attention to the demixing transition, by applying a depletion picture on the theoretical side and

measurements of the correlation length of the mixtures on the experimental side, thus providing evidence for demixing that compares well with the theoretical predictions. The combined results are discussed and put in a broader context in Section 5, whereas in Section 6 we summarize and draw our conclusions.

2 Methods

2.1 Coarse-grained model

We analyze the properties of mixtures of star polymers and colloidal additives in the limit in which the colloids are smaller than the polymers. The theoretical approach used to describe the system is based on a previously introduced coarse-grained representation. [34,41] Star polymers are macromolecular colloidal species consisting of a number f of homopolymers grafted on a central core. They can be regarded as soft spherical colloids with a gyration radius $R_S^{(g)}$ scaling as $R_S^{(g)} \sim f^{1/5} N^\nu$ under good solvency conditions, [42] where N is the degree of polymerization per arm, f the arm number (functionality) and $\nu = 0.588 \simeq 3/5$ the self-avoiding Flory exponent. The second component of the mixtures are colloids, i.e., hard spherical nanoparticles with radius R_H. Each species is rendered as a spherical object (soft and hard, respectively) and coarse-grained through its center. Accordingly, we introduce effective potentials $V_{ij}(r)$ $(i, j = S, H)$ acting between the sphere centers at distance r.

The effective interaction potential $V_{SH}(r)$ between star polymers and hard colloids in good solvent conditions depends on f and on the size ratio q, defined as:

$$q \equiv R_S^{(g)}/R_H, \tag{1}$$

whereby we focus here exclusively on the case $q > 1$. The coarse-graining procedure allows the extraction of the effective force between the star polymer and the colloid by integrating the osmotic pressure $\Pi(s)$ exerted by the star polymer on the surface of the colloid. [34,41] In this way, the effective force $F_{SH}(z)$ between the anchor point of the star and the surface of the hard colloid can be evaluated as

$$F_{SH}(z) = \frac{R_H}{(z+R_H)^2} \int_z^{s_{max}} ds \left[z^2 + 2R_H z + s^2\right] \left[\Pi(s) - \Pi(s+t)\right], \tag{2}$$

where $z = r - R_H > 0$ is the distance from the center of the star to the surface of the hard colloid, $s_{max} = \sqrt{z(z+2R_H)}$ and $t(s) = \left(z(2R_H + z) - s^2\right)/s$. The functional form of the osmotic pressure $\Pi(s)$ can be found in Refs. [34,41]; for the numerical coefficient $\Lambda(f)$ appearing there, the high-f-limit $\Lambda(f) = 5/36$ has been employed in this work for all $f \geq 200$. We note that the results for the structure of the mixtures are rather insensitive to the precise value of $\Lambda(f)$, even within a factor of 2 to 3. The effective force can be readily integrated to yield the theoretical prediction for the effective potential $V_{SH}(r = R_H + z)$, the validity of which was firmly corroborated via extensive, full-monomer Monte-Carlo simulations. [41]

Within the coarse-grained representation the interaction between hard colloids, $V_{HH}(r)$, is represented by the hard sphere
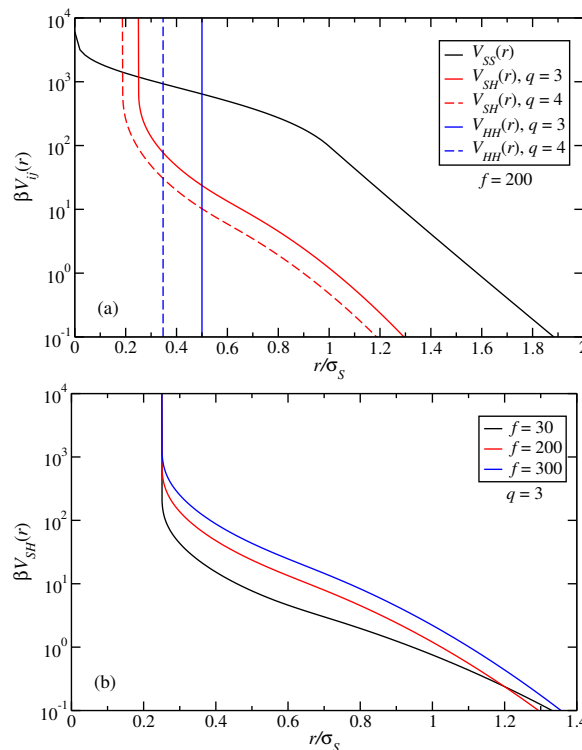
Fig. 1 (a) The effective interactions between star-star, $V_{SS}(r)$, star-colloid, $V_{SH}(r)$, and colloid-colloid, $V_{HH}(r)$, for star functionality $f = 200$ and size ratios $q = 3$ (solid lines) and $q = 4$ (dashed lines). The colloid-colloid interactions are of the hard-sphere type and are thus represented here by vertical lines. (b) The cross-interaction $V_{SH}(r)$ for fixed size ratio $q = 3$ and varying functionality f of the star.

potential for particles with diameter $\sigma_H = 2R_H$,

$$\beta V_{HH}(r) = \begin{cases} \infty & r < \sigma_H; \\ 0 & r \geq \sigma_H. \end{cases} \tag{3}$$

Finally, for the star-star effective interaction, $V_{SS}(r)$, the effective potential derived in Ref. [16] was employed. The latter features a crossover from a Yukawa-like tail to a logarithmic behavior as the star-star separation diminishes. More explicitly, the effective interaction between two star-polymers whose centers are held at distance r apart reads as

$$\beta V_{SS}(r) = \frac{5}{18} f^{3/2} \begin{cases} -\ln\left(\frac{r}{\sigma_S}\right) + \frac{1}{1+\sqrt{f}/2} & r < \sigma_S \\ \frac{1}{1+\sqrt{f}/2} \left(\frac{\sigma_S}{r}\right) \exp\left[-\frac{\sqrt{f}}{2\sigma_S}(r-\sigma_S)\right] & r \geq \sigma_S \end{cases} \tag{4}$$

where $\sigma_S \simeq (4/3) R_S^{(g)}$ is the corona diameter of the stars and $\beta = (k_B T)^{-1}$, k_B being the Boltzmann constant and T the absolute temperature. All the effective potentials used in this work are fully repulsive and arise in systems whose only microscopic interactions are excluded volume effects. The set of effective interactions given by Eqs. (2-4) was employed to investigate the structural and dynamic features of mixtures characterized by high functionalities $f = 214, 250, 300$ and size ratios $2 \leq q \leq 8$. The theoretical modeling will be mostly performed in concentration regimes in which there is no osmotic shrinkage of the stars due to either other stars or the colloids; [43] therefore the inter-

action parameter σ_S as well as the size ratio will be treated as concentration-independent constants.

In Fig. 1, some examples of the effective interactions are shown for different f and two size ratios q. Since the colloids are considered as hard spheres, the star-colloid interaction $V_{SH}(r)$ diverges at $r = R_H$ and, as expected, it also diverges at smaller distances for larger q, since smaller colloids can penetrate the stars more easily than larger ones. For a given q, the stars become less penetrable by the colloids as the functionality of the star increases. In this way, this reliably determined set of effective potentials provides full and realistic coarse-graining of the complex mixture.

2.2 Experimental techniques

2.2.1 Sample preparation

Suspensions of multi-arm 1,4-polybutadiene (PBD) star polymers with a weight-average functionality $f_S \equiv f = 214$ arms, having a total weight-average molar mass $M_{w,S} = 14400 \, \text{kg/mol}$ were treated as the experimental counterpart to the theoretical soft-colloids presented the previous sections. In order to suppress any enthalpic contribution coming from the eventual difference of chemical composition between hard colloids and stars that could dictate the thermodynamic behavior of the mixtures, smaller PBD stars with a higher functionality $f_H = 1110$ and total $M_{w,H} = 1410 \, \text{kg/mol}$ were considered as effective hard-sphere colloidal particles. This choice is justified by the $(f \to \infty)$-limit of the coarse-grained star-star interaction (see Eq. (4)).[16,36] Details on the synthesis and the characterization of the stars are provided in Refs.[36,44,45]. The mixtures of stars and hard-like spheres were dissolved in squalene, a nearly athermal, non-volatile solvent for PBD.

2.2.2 Dynamic light scattering

Dynamic light scattering (DLS) measurements were performed using the Photon Correlation Spectroscopy (PCS) technique,[46] which recorded the scattering intensity autocorrelation function $G(Q,t) = \langle I(Q,t)I(Q)\rangle / |I(Q)|^2$ over a broad time range ($10^{-7} - 10^3$ s) at different scattering wave vectors Q with an ALV-5000 goniometer/correlator setup (ALV, Germany) using a Nd:YAG laser at wavelength $\lambda = 532 \, \text{nm}$ (Adlas, Germany). The magnitude of the scattering wavevector is $Q = (4\pi n/\lambda)\sin(\theta/2)$ where n and θ are the refractive index of the solvent and the scattering angle, respectively. We performed measurements in the polarized (VV) geometry under homodyne beating conditions. The intermediate scattering function $C(Q,t)$ probing concentration fluctuations was extracted from the experimental intensity autocorrelation function acquired at the photomultiplier tube, $G(Q,t)$, viz:

$$C(Q,t) = \left[\frac{G(Q,t)-1}{f_{\text{ins}}^*}\right]^{1/2}, \tag{5}$$

where $f_{\text{ins}}^* \leq 1$ is an instrumental coherence factor.

The analysis of $C(Q,t)$ was performed using the CONTIN software[47] and proceeded by its inverse Laplace transformation (ILT)

$$C(Q,t) = \int_{-\infty}^{\infty} L_Q(\ln\tau) \exp(-t/\tau) \, \text{d}\ln\tau, \tag{6}$$

$L_Q(\ln\tau)$ being the distribution of relaxation times for a given wave vector Q. This was particularly useful for higher concentrations, where more than one relaxation mode could be detected. However we point out that all the DLS data reported hereafter refer to samples laying below the glass line of the colloid-free system, where samples are ergodic and spatial average of the scattering intensity is not necessary to characterize their structural relaxation. A single exponential relaxation process was observed for dilute solution analysis, from which the hydrodynamic radii were extracted. The hydrodynamic radii of the soft and hard colloids, measured in dilute squalene solution at $20°\text{C}$, were $R_S^{(h)} = 45 \, \text{nm}$ and $R_H^{(h)} = 11.5 \, \text{nm}$, respectively, which yields a colloid-to-star hydrodynamic size ratio $\zeta = R_H^{(h)}/R_S^{(h)} \simeq 0.25$ and overlap concentrations $c_S^* = 44.5 \, \text{mg/ml}$ and $c_H^* = 416 \, \text{mg/ml}$. Since $R_S^{(h)} \simeq \sigma_S$ for multiarm stars,[23,36] and also $\sigma_S \simeq 4R_S^{(g)}/3$, it follows that $q = 3/(4\zeta)$ and thus the size ratio $q = 3$ is obtained for the system being considered. Based on single particle hydrodynamic sizes, we also estimated the nominal effective volume fractions for rheological glass transitions to be $\phi_S^{(g)} = c_S^{(g)}/c_S^* = 1.61$ for the stars, corresponding to $\rho_S^{(g)}\sigma_S^3 = 0.327$, and $\phi_H^{(g)} = c_H^{(g)}/c_S^* = 0.75$ for the colloids, meaning $\rho_H^{(g)}\sigma_S^3 = 10.75$.[36]

In the DLS experiment one can measure both the dynamics (relaxation rate) and the intensity of a relaxation mode. Since we make use of both, below we call this static/dynamic light scattering. In addition to standard DLS we performed Multispeckle dynamic light scattering (MSDLS) experiments for two non-ergodic samples at $\phi_S = 1.625$ and two different colloid concentrations, i.e. samples that explore only a limited portion of the phase space on the experimentally accessible time scales. For such samples, the time average usually applied to measure $G(Q,t)$ is practically unfeasible. To circumvent this difficulty we use the multispeckle method.[48,49] A multi-pixel CCD camera is used as a detector, instead of a single detector such as a phototube, as in traditional light scattering. The signal of each pixel is treated independently and the intensity correlation function is averaged over pixels, rather than over time. More specifically, we calculated $G(Q,t)$ as:

$$G(Q,t) = \left\langle \frac{\langle I_p(Q_p, \tau+t)I_p(Q_p, \tau)\rangle_p}{\langle I_p(Q_p, \tau+t)\rangle_p\langle I_p(Q_p, \tau)\rangle_p} \right\rangle_\tau \tag{7}$$

where $I_p(Q_p,t)$ is the intensity at time t for the p-th pixel, Q_p is the scattering vector associated to the light collected by the p-th pixel and $\langle\ldots\rangle_p$ denotes an average over CCD pixels corresponding to a set of Q-vectors centered in $Q = 22.2 \, \mu\text{m}^{-1}$ and such that the relative change of Q over the pixels is $\Delta Q/Q < 0.1$. We estimate the experimental observational length scale as $2\pi/Q = 282$ nm $\simeq 6\sigma_S$: we thus probe collective diffusion. No significant ageing was detected, and the time average yielded the usual $G(Q,t) - 1$, proportional to the squared intermediate scattering function that quantifies the temporal decay of density fluctuations of wave vector Q.[46]

2.2.3 Rheology

The linear and nonlinear viscoelastic responses of the star mixtures were measured under simple shear flow. The measurements were performed with a sensitive strain-controlled ARES

Soft Matter Accepted Manuscript

100 FRTN1 rheometer (TA, USA) employing a homemade cone-plate stainless steel geometry (diameter = 7.9 mm, cone angle = 0.166 rad, truncation = 0.210 mm), in order to accommodate minimal amounts of samples. The temperature was maintained at $20.00 \pm 0.01^\circ$ C with a Peltier control system, whereas the sample was protected from the external environment with a simple teflon cover.

The experimental protocol involved the following dynamic oscillatory measurements: (a) Strain sweeps at frequency $\omega = 1$ rad/s, to determine the limits of linear viscoelastic response. (b) Time sweeps at large strain amplitude $\gamma_0 = 200\%$ and frequency $\omega = 1$ rad/s, to shear-rejuvenate the sample (or shear-melt it when solid-like), typically for $t_{rej} = 10^2$ s. This protocol allowed erasing the sample history (due to possible residual stresses during sample preparation and loading) and ensured reproducible initial conditions for the measurements.[36] This approach was used consistently in all the measurements. (c) Time sweeps at low, linear γ_0 ($\gamma_0 < 1\%$), to monitor the aging of the sample and determine its rheological steady state. The latter is particularly important over periods exceeding $t_{ag} = 10^4$ s.[36] (d) Frequency sweeps at strain $\gamma(t) = \gamma_0 \sin(\omega t)$, to probe the viscoelastic relaxation spectrum, i.e., the frequency-dependent storage (G') and loss (G'') moduli in the range $10^{-2} - 10^2$ rad/s. The measured stress response is $\tau(t) = \tau_0 \sin(\omega t + \delta) = \gamma_0 (G' \sin \omega t + G'' \cos \omega t)$, τ_0 being the stress amplitude and δ the phase angle $\delta = \tan(G''/G')$.

3 Glass melting and reentrance

3.1 Static structure

Using the set of effective interactions defined above to describe the system defined, we proceed to the analysis of the static structure of the mixtures characterized by partial number densities $\rho_i = N_i/V$ $(i, j = S, H)$. To determine the correlation functions between the two species, we employed integral equation theories and tested their accuracy by Monte Carlo simulations of the coarse-grained system at selected points. The two-component Ornstein-Zernike equation was solved with the help of the Rogers-Young closure (OZ-RY).[50] In Fourier space, the former reads as

$$\hat{\mathbf{H}}(Q) = \hat{\mathbf{C}}(Q) + \hat{\mathbf{C}}(Q) \cdot \hat{\mathbf{D}} \cdot \hat{\mathbf{H}}(Q), \qquad (8)$$

where $[\hat{\mathbf{H}}(Q)]_{ij} = \hat{h}_{ij}(Q)$ and $[\hat{\mathbf{C}}(Q)]_{ij} = \hat{c}_{ij}(Q)$ are, respectively, the Fourier transforms of the total and the direct correlation functions, and $[\hat{\mathbf{D}}]_{ij} = \rho_i \delta_{ij}$.

To find a solution for Eq. (8) it is necessary to make use of additional closure relations. In this work, the two-component Rogers-Young closure was chosen, as it is known to give thermodynamically consistent results for mixtures of star polymers and hard colloidal particles.[51] The RY closure relation is given by

$$g_{ij}(r) = \exp[-\beta V_{ij}(r)] \left(1 + \frac{\exp[f_\alpha(r)\gamma_{ij}(r)] - 1}{f_\alpha(r)} \right), \qquad (9)$$

where $g_{ij}(r) = h_{ij}(r) + 1$ is the radial distribution function, $V_{ij}(r)$ is the pair interaction potential, and $\gamma_{ij}(r) = h_{ij}(r) - c_{ij}(r)$. The mixing function $f_\alpha(r) = 1 - \exp(-\alpha r)$ enforces thermodynamic consistency of the compressibility and the virial routes by tuning the parameter α.[50] By iteratively solving Eqs. (8) and (9), we calcu-
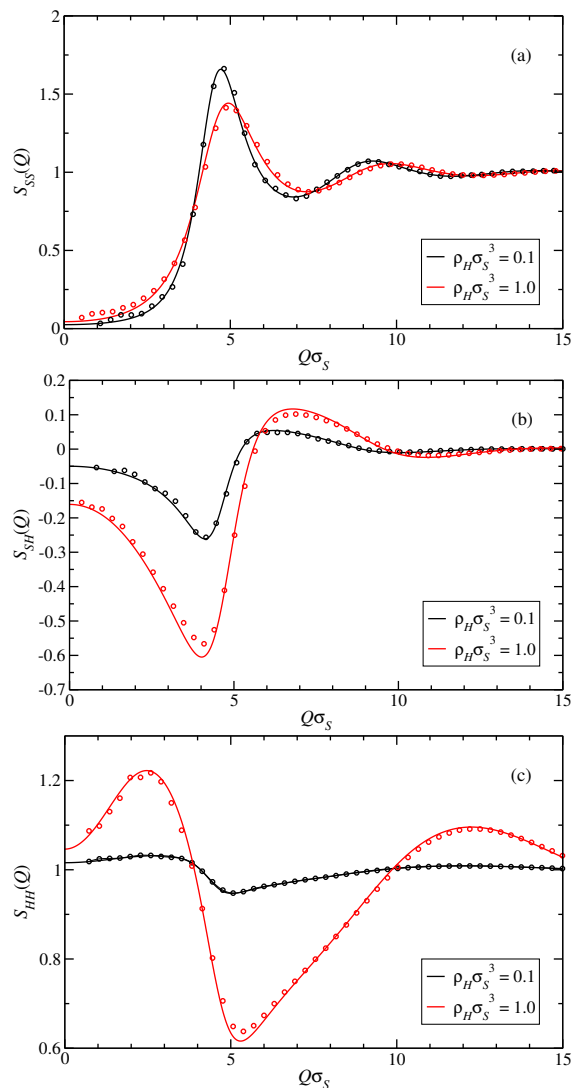
Fig. 2 Partial structure factors obtained from the solution of the OZ-RY equation (lines) and Monte-Carlo simulations (symbols) for $f = 30$, $q = 3$, $\rho_S \sigma_S^3 = 0.3$, and two different colloidal densities, $\rho_H \sigma_S^3 = 0.1$ and 1.0, as indicated in the legends.

lated the radial pair distribution functions $g_{ij}(r) = h_{ij}(r) + 1$, and the static structure factors $S_{ij}(Q) = \delta_{ij} + \sqrt{\rho_i \rho_j} \hat{h}_{ij}(Q)$ for different functionalities f, size ratios q and reduced partial densities $\rho_H \sigma_S^3$ and $\rho_S \sigma_S^3$. Representative results are shown in Figs. 2 and 3.
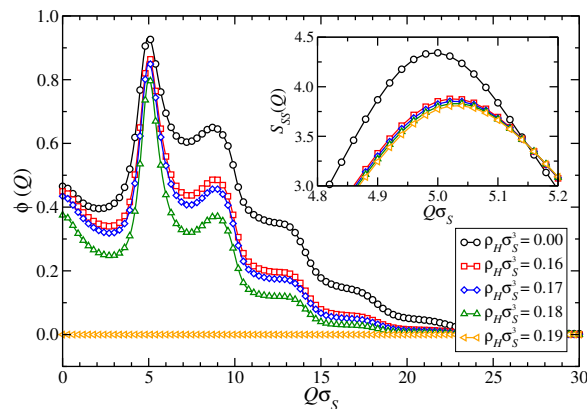
In Fig. 2 we show the dependence of the partial structure factors for $f = 30$, $q = 3$ and $\rho_S \sigma_S^3 = 0.30$ on the density of the colloidal additives. As the colloidal density ρ_H increases, the main peak of $S_{SS}(Q)$ diminishes in height and its location shifts to larger wavenumbers; increasing the colloidal density thus reduces the the star-star nearest-neighbor distance, while at the same time it also "loosens" the correlations between the stars. Due to the presence of the colloids, the stars overlap more frequently, they penetrate deeper into each other, i.e., they are "pushed together" by the colloids. This is a typical depletion effect, present for all functionalities. In fact, the colloid-induced depletion can drive the system to a demixing instability, as implied by the structural data for $f = 250$ in Fig. 3. We can see that even for a small amount of
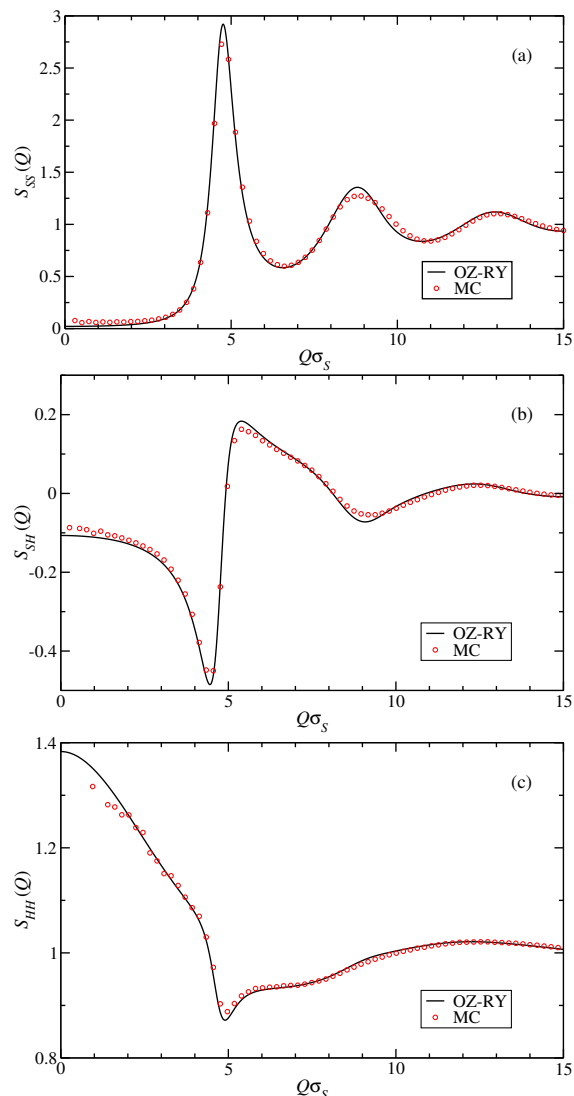
Fig. 3 Partial structure factors obtained from the solution of the OZ-RY equation and Monte-Carlo (MC) simulations for $f = 250$, $q = 3$, $\rho_S \sigma_S^3 = 0.3$, and $\rho_H \sigma_S^3 = 0.1$.

Fig. 4 Dependence of the non-ergodicity factor on the density of added colloids for $f = 214$, $q = 3$, and $\rho_S \sigma_S^3 = 0.36$. Inset: Close-up to the main peak of the corresponding star-star structure factors.

additives, $\rho_H \sigma_S^3 = 0.1$, the colloid-colloid structure factor $S_{HH}(Q)$ develops a high peak for long wavelengths ($Q \to 0$) signaling that the system is approaching the spinodal line, and therefore, phase separation would take place for further increase of ρ_H.

The possible existence of a demixing region can be accounted for by the well-known fact that in the neighborhood of a spinodal line, iterative schemes as OZ-RY fail to converge.[50] In this way, an estimate of the phase-separated region can be obtained by locating the convergence line, i.e., set of points $(\tilde{\rho}_S, \tilde{\rho}_H)$ above which the homogeneous mixture is expected to become unstable with respect to a demixing transition into colloid-rich and star-rich fluid phases. At this point, Figs. 2 and 3 indicate that increasing the functionality of the star results in a stiffer particle, which is less penetrable for the colloidal additive and yields demixing at lower concentration of the latter, as can be concluded by comparing the values of $S_{HH}(Q \to 0)$ for $\rho_H \sigma_S^3 = 0.1$.

3.2 Mode Coupling Theory

According to the Hansen Verlet criterion, stating that a liquid will freeze when the main peak of $S(Q)$ reaches a height above 2.8, the pure, star polymer fluid would crystallize, i.e., a thermodynamic fluid-solid transition might take place at high star concentrations (see Fig. 3 and inset in Fig. 4). However several experimental studies have shown that a transition to a disordered arrested state (glassy state) is what actually happens rather than crystal nucleation.[24,52,53] To quantify the extent to which this glassy state is affected by the addition of small, hard colloids, we focused on the non-ergodicity factor $\phi(Q)$ of the stars, which is defined as the long-time limit of the star-star density autocorrelation function. In the case $\phi(Q) \neq 0$, the system is considered non-ergodic and its state is identified as glassy, whereas $\phi(Q) = 0$ corresponds to an ergodic fluid.

Given the structural data obtained by the OZ-RY approach, the calculation of the non-ergodicity factor is readily achieved within the framework of the Mode Coupling Theory (MCT). According to MCT, $\phi(Q)$ fulfills the self-consistent equation:[50,54,55]

$$\frac{\phi(Q)}{1 - \phi(Q)} = \frac{1}{(2\pi)^3} \int d^3 k \, \mathscr{V}(\mathbf{Q}, \mathbf{k}) \phi(k) \phi(k'), \quad (10)$$

where $\mathbf{k}' = \mathbf{Q} - \mathbf{k}$ and the kernel $\mathscr{V}(\mathbf{Q}, \mathbf{k})$ can be expressed entirely in terms of structural data, i.e.,

$$\mathscr{V}(\mathbf{Q}, \mathbf{k}) = \frac{\rho S(Q)}{2Q^4} \left[(\mathbf{Q} \cdot \mathbf{k}') \hat{c}(k') + (\mathbf{Q} \cdot \mathbf{k}) \hat{c}(k) \right]^2 S(k) S(k'), \quad (11)$$

and $S(Q) = [1 - \rho \, \hat{c}(Q)]^{-1}$.

We evaluated $\phi(Q)$ using as inputs the star density and the star-star structure factor resulting from the solution of the OZ-RY equation, i.e., $S(Q) \equiv S_{SS}(Q)$ for a given set $\{f, q, \rho_S, \rho_H\}$ and $\rho \equiv \rho_S$. Focusing exclusively on the dynamics of the large component is justified when the size discrepancy and the concomitant asymmetry in the short-time mobilities of the two components is large enough.[56] We have explicitly checked that this is indeed the case for the system at hand.[36] A representative result of the dependence of the non-ergodicity factor of the stars on the colloidal additive is shown in Fig. 4, for the experimentally relevant
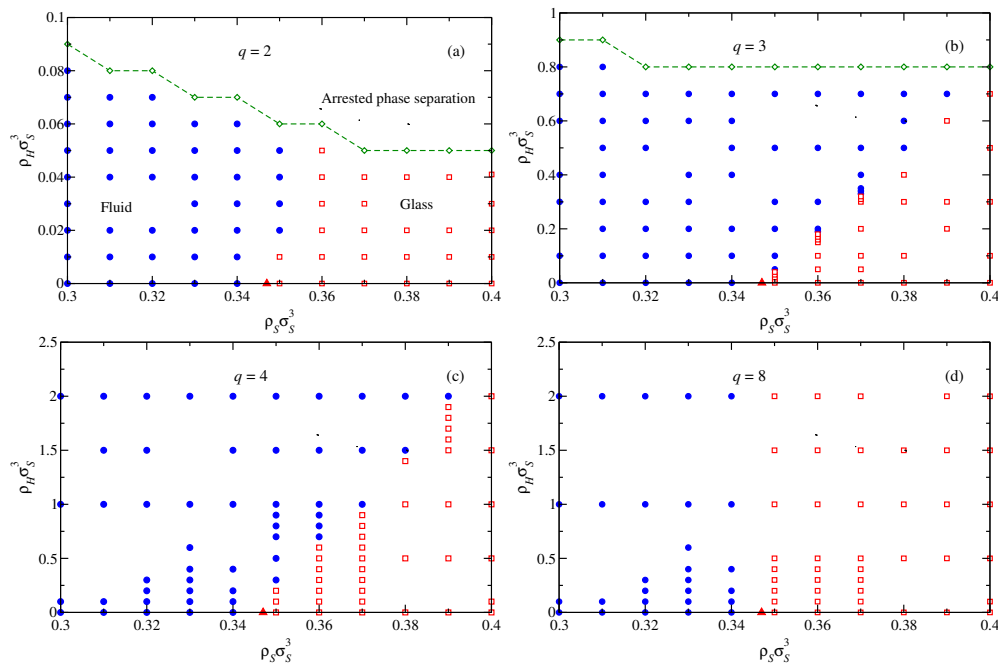
Fig. 5 Mixture state diagram for $f = 214$ and different size ratios q as indicated in the legends. Panel (b) corresponds to the system that has also been analyzed experimentally. The blue circles mark ergodic fluid states while the red squares represent glassy states. The filled triangles indicate the liquid to glass transition density $\rho_S^{(g)}$ for the pure star system. The dashed line corresponds to the convergence line above which the mixture is considered to undergo an arrested phase separation, as explained in the main text.
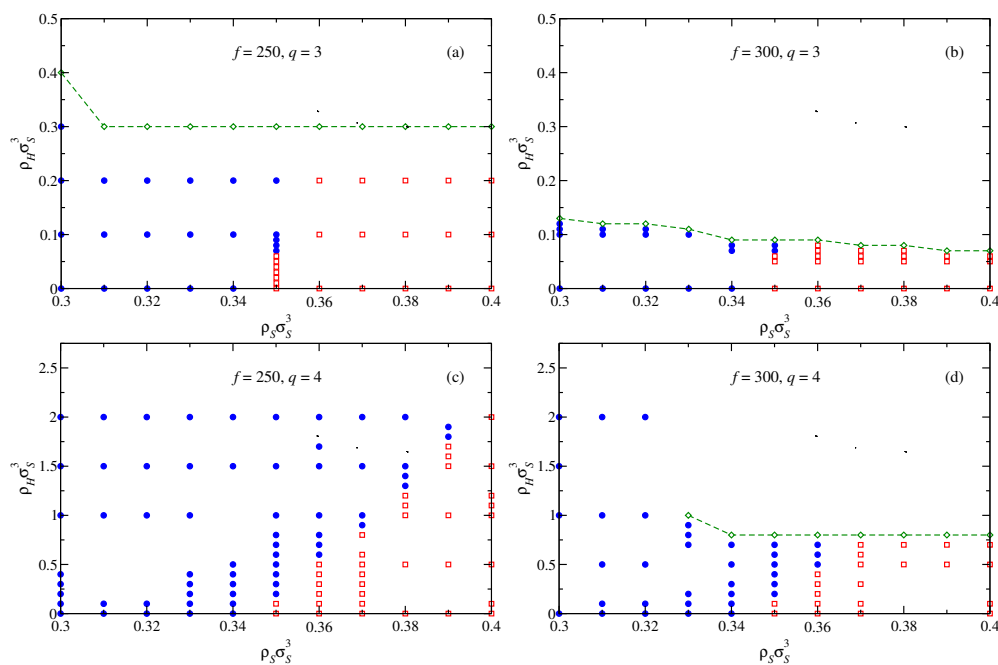
Fig. 6 Mixture state diagrams for $f = 250$ and $f = 300$ and different size ratios, as indicated in the legends. The blue circles correspond to ergodic fluid states while the red squares represent glassy states. Above the dashed line, the systems is considered to undergo an arrested phase separation.

combination $f = 214$, $q = 3$, $\rho_S\sigma_S^3 = 0.36$ and increasing colloidal density. Upon the addition of the colloids, the star-star structure weakens and for $\rho_H\sigma_S^3 \gtrsim 0.18$ the glass melts and ergodicity is restored. As more hard colloids penetrate the stars, the cages of the repulsive star glass are perturbated and finally broken leading to melting of the system.

A compilation of results for various combinations of partial densities and size ratios at fixed star functionality $f = 214$ is provided in Fig. 5, which shows the thus obtained state diagrams for the binary mixtures. For the pure star system, the (MCT) fluid-to-glass transition takes place at $\rho_S^{(g)}\sigma_S^3 \simeq 0.347$. For larger star densities, the addition of colloids leads to melting of the glassy state as

previously described, the effect being more pronounced for size ratios $q = 3$ and $q = 4$. The smaller the additive, i.e., the higher q, the larger the colloid concentration necessary before melting takes place. In particular, for $q = 8$ no change is observed in the state of the pure star system at a given ρ_S, which leads to the conclusion that such mixtures of large star polymers and very small, hard additives form a stable binary nanocomposite within the density range considered. This is physically reasonable, since in this case the small (hard) colloids can penetrate into the stars with a very small free energy penalty and hardly affect the structure of the soft (large) colloids.

On the other hand, when size ratios $q = 2$ and $q = 3$ are considered, a non-convergence region is found when solving the OZ-RY equation for larger colloidal densities. As mentioned above, the locus of points $(\tilde{\rho}_S, \tilde{\rho}_H)$ where this firstly happens can be regarded as a reasonable estimate of the demixing line.[50] In this way, systems with $\rho_S \gtrsim \rho_S^{(g)}$ and ρ_H within the non-convergence region will very likely undergo an arrested phase separation, as indicated in Fig. 5, inasmuch as an interplay between phase separation and glass formation will occur under these conditions.[37–40]

The described trends are very similar for mixtures characterized by higher functionalities, as demonstrated in Fig. 6 for $f = 250$ and $f = 300$. The features of these systems resemble those of the $f = 214$ case but they markedly differ in the lower colloidal density range at which demixing commences for $q = 3$ and $q = 4$. Again, this can be rationalized as an effect of the lower penetrability of stars for higher f, rendering $V_{SH}(r)$ more repulsive (see Fig. 1), and consequently favoring earlier demixing as ρ_H grows. Accordingly, the region in which the addition of colloids leads to melting of the star-polymer glass becomes narrower for increasing f, in the sense that although smaller ρ_H will melt the glass at a fixed $\rho_S > \rho_S^{(g)}$, as can be verified by comparing Fig. 5 and 6 for the case $q = 4$, the demixing line will move to lower colloidal densities. This is most characteristically seen for the case $f = 300$ and $q = 3$ in Fig. 6(b). As q increases, the star functionality becomes irrelevant: For $q = 8$ the state diagram looks exactly the same for the three functionalities investigated without signals of glass melting or phase separation, whereas for $q = 2$ the system demixes immediately for $f = 250$ and $f = 300$ when colloidal particles are added. We will rationalize these findings in Section 4.1 by employing a depletion picture.

3.3 Experimental Results

3.3.1 Linear viscoelastic response of the mixture

Representative results of linear viscoelastic spectra are presented in Fig. 7, where storage (G') and loss (G'') moduli are depicted for samples with $f = 214$ and $q = 3$ at fixed star fraction $\phi_S = 1.625 > \phi_S^{(g)}$ $\left(\rho_S \sigma_S^3 = 0.343\right)$ and varying colloid densities. In the figure, moduli are normalized by $k_B T \left[R_S^{(h)}(\rho_H) \right]^{-3}$ taking into account the dependence of the star hydrodynamic radius on the increasing colloid fraction, as discussed in Section 3.3.2. As can be noted, (non-ergodic) solid-like states are found for colloid densities $\rho_H \sigma_S^3 = 0.029$, 2.375 and 5.892, while an ergodic liquid-like state is reached at $\rho_H \sigma_S^3 = 0.442$. The three solid-like states exhibit qualitatively similar behavior with $G' > G''$ over the whole
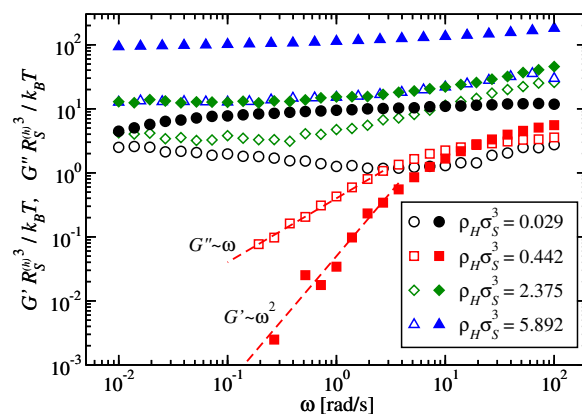

Fig. 7 Linear viscoelastic spectra of star-colloid mixtures with $f = 214$ and $q = 3$ at $\phi_S = 1.625$ $(\rho_S \sigma_S^3 = 0.343)$ and different colloid fractions, which feature different rheological states. Normalized storage (G') and loss (G'') moduli are shown with full and empty symbols, respectively. Representative examples are plotted for repulsive glass ($\rho_H \sigma_S^3 = 0.029$), liquid ($\rho_H \sigma_S^3 = 0.442$), reentrant glass attributed to arrested phase transition ($\rho_H \sigma_S^3 = 2.375$), and reentrant double glass ($\rho_H \sigma_S^3 = 5.892$). Dashed lines indicate terminal moduli slopes for the liquid sample (see main text).

frequency range probed in the experiment, with a plateau G', and with G'' going through a minimum around 2, 0.4, and 0.2 rad/s for increasing colloid concentration, respectively.

For the lowest colloid density the sample shows the typical behavior of a repulsive glass, which melts by the addition of colloids. This intermediate liquid state exhibits moduli which tend to reach the plateau modulus of the repulsive glass at high frequencies, whereas at lower frequencies they comply with the viscoelastic liquid scaling $G' \sim \omega^2$ and $G'' \sim \omega$ (Fig. 7). By further increasing the colloid concentration, the mixture undergoes a reentrant transition to a solid-like state attributed to arrested phase separation (APS), which features G' and G'' close to the moduli of the repulsive glass at low frequency. On the other hand, at higher colloid density the reentrant glass has moduli exceeding those of the repulsive glass by almost one decade each. As discussed below, this state resembles a double glass formed by a binary mixture of hard spheres.

A more detailed description of the sequence of states of the mixture as the colloid concentration increases is provided by the effective plateau modulus G_p shown in Fig. 8. At low colloid density, a repulsive-glass region is characterized by non-monotonic dependence of G_p on colloid concentration due to the competition between reinforcement and depletion: initially the addition of hard spheres has a reinforcing effect on the stars, but with further colloid addition depletion takes place and the modulus decreases while the mixture remains glassy. An additional increase in ρ_H leads to an intermediate depletion-induced liquid region (glass melting), in full agreement with the results from MCT, in which also colloid-induced melting of the star glass has been seen. The characteristic time of the liquid (extracted from the terminal crossover of the moduli, i.e., $\tau = 1/\omega_{\text{crossover}}$) varies over three decades; it first decreases with ρ_H, then goes through a minimum and finally increases as the reentrance is approached. As the colloid concentration is further increased ($\rho_H \sigma_S^3 \gtrsim 1.0$) a re-entrant,
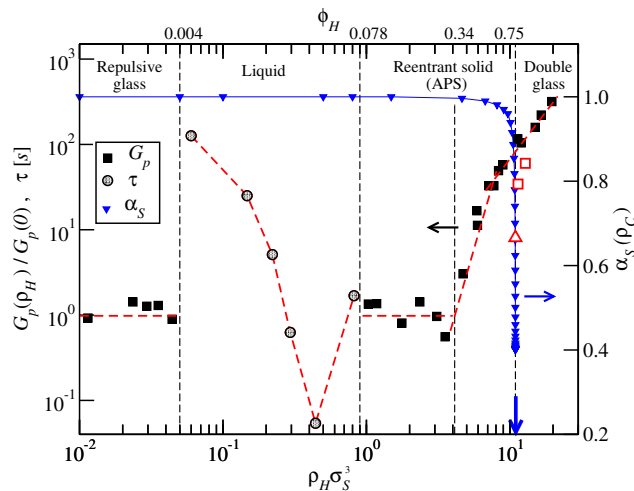
Fig. 8 Left vertical axis: Normalized plateau modulus (G_p, squares) of the arrested states and relaxation time (τ, circles) of the ergodic phase of the mixture as a function of the colloid concentration at $\phi_S = 1.625$ ($\rho_S \sigma_S^3 = 0.343$). Vertical dashed lines separate the different states identified by rheology and are located at the colloid volume fraction ϕ_H indicated in the upper horizontal axis. Vertical blue arrow marks the (rheological) glass transition concentration ($\phi_C^{(g)} = 0.75$, $\rho_H \sigma_S^3 = 10.75$) for pure solutions of small hard colloids; for the latter, the empty red squares indicate the measured G_p at $\phi_H = 0.79$ and 0.89. The empty red triangle pinpoints the fluctuation-dissipation estimate of the plateau modulus $G_{p,HS} = k_B T / [R_H^{(h)}]^3$ for hard-spheres at the (ideal) glass transition. Dashed red lines are a guide to the eye. Right vertical axis: Shrinkage factor in squalene for the soft stars (α_S, blue triangles) as a function of colloid density calculated according to Eqs. (12)-(14).

solid-like regime is found, which can be identified with arrested phase separation as theoretically predicted (see discussion above) and which, in turn, is characterized by different regions, potentially marking solid-solid transitions.[36]

As previously reported,[36] the lower colloid fraction within the re-entrant regime ($1 \lesssim \rho_H \sigma_S^3 \lesssim 4$), the system exhibits a two-step yield process reflecting two constraining length scales that occur both in attractive glasses and in arrested phase separating systems.[57] However, in this region the plateau modulus G_p is virtually independent of ρ_H and nearly identical to that of the repulsive glass, as can be seen in Fig 8. The latter feature is inconsistent with attractive vitrification, where a much higher storage modulus would be expected, ruling out this possibility in favor of the APS scenario. With further addition of hard spheres ($\rho_H \sigma_S^3 > 4$), the modulus increases rather dramatically following two distinct power laws (see Fig. 8). This behavior sets mixtures based on soft colloids apart from their hard sphere counterparts. We attribute this to the deformability of the soft colloids due to the presence of an increasingly crowded hard spheres environment. To elucidate this behavior in a quantitative fashion, we analyzed the osmotic effects of the small colloids on the stars.

3.3.2 Effect of star shrinkage

Our starting point is the osmotic shrinkage undergone by one star polymer with radius R_S due to the addition of a smaller colloidal additive with size R_H and a packing fraction η_H.[43] In such case, the minimization of the free energy imposes the following equi-

librium condition with respect to the star radius R_S:

$$\frac{fR_S}{Na^2} - v_0 \frac{N^2 f^2}{2R_S^4} + \frac{R_S^2}{R_H^3}\eta_H Z(\eta_H) = 0, \qquad (12)$$

where N is the polymerization degree of each arm of the star, a is the monomer size ($a = 0.5$ nm for PBD[58]), v_0 is the excluded volume parameter that can be set equal to a^3, and $Z(\eta)$ is the compressibility factor of the colloidal bath. For the case of hard colloids, it takes the form[59]

$$Z(\eta) = \begin{cases} \frac{1+\eta+\eta^2-\eta^3}{(1-\eta)^3} & \eta < \eta^{(g)} \\ \frac{2.67}{1-1.543\eta} & \eta > \eta^{(g)} \end{cases} \qquad (13)$$

where $\eta^{(g)} = 0.58$ is the packing fraction at the glass transition for hard spheres. Note that here the volume fraction of hard spheres has been calculated as $\eta_H = V_H / (V_{solv} + V_H)$. The normalized colloid concentration may then be expressed as a function of the known experimental parameters:

$$\rho_H \sigma_S^3 = \frac{3}{4\pi}\left(\frac{R_S}{R_H}\right)^3 \left[1 - \left(\frac{3}{4\pi R_S^3}\frac{M_{w,S}}{N_A \rho_{PBD}}\right)\phi_S\right]\eta_H \qquad (14)$$

where $R_S \equiv R_S^{(h)}$ is the hydrodynamic radius of the soft star at infinite dilution, $\phi_S = c_S/c_S^* = 1.625$, and ρ_{PBD} is the density of polybutadiene. Equations (12)-(14) were employed in a fully self-consistent fashion to calculate the star shrinkage factor $\alpha_S = R_S^{(h)}(\rho_H)/R_S^{(h)}$ as function of the colloid density $\rho_H \sigma_S^3$. We expect this to be accurate even if the presence of more stars (overlapping) was not considered in Eq. (12).

As can be seen in Fig. 8, the modulus G_p increases significantly from a colloid fraction $\rho_H \sigma_S^3 \sim 4$, when the star size starts decreasing (albeit weakly). Moreover, a slope change for G_p occurs at a colloid fraction $\rho_H \sigma_S^3 \sim 8$, when the size of the stars (and hence their osmotic pressure) is reduced appreciably. Note that the star radius can drop continuously up to the limit of star collapse,[42] i.e. when a star reaches its hard-like compact shape and $R_S \sim a(fN)^{1/3}$. In the present case the collapsed R_S is about 16 nm, i.e., slightly above the colloid size. At such high colloid concentrations, the soft stars become dramatically squeezed and assume a collapsed configuration akin to that observed under poor solvency conditions. Accordingly, they can also be thought of as hard spheres that are slightly larger than the original colloids. The system, under these conditions is thus very similar to a slightly asymmetric binary hard sphere mixture. The overall packing fraction can be estimated to lie very close to the glass transition packing fraction of the hard-sphere system, marked by the vertical arrow in Fig. 8. Therefore we interpret this new solid as a glass formed by a binary hard sphere mixture and we call it a double glass, in accordance with the general terminology of multiple glasses for such systems.[19,20,60] In contrast to the star polymer glass encountered at lower concentrations of colloidal particles, in which the stars are arrested but the colloids are mobile,[36] in this double-glass both components are mutually caged. We point out here that double glass is the only feature of the experimental state diagram that cannot be captured by the theoretical diagram

(Fig. 5b), since the present analysis does not take into account the star shrinkage.
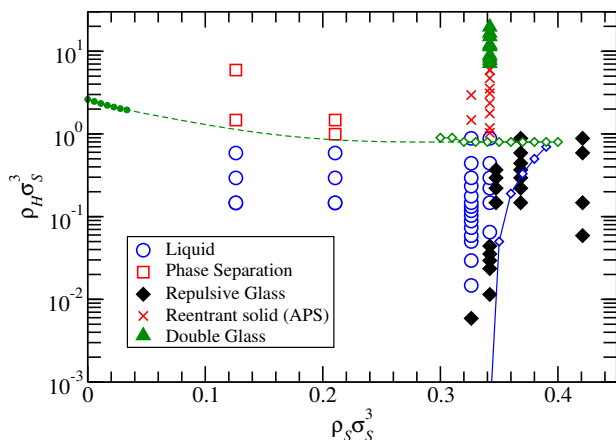

Fig. 9 State diagram of star polymer-colloidal mixtures for $f = 214$ and $q = 3$ extracted from the linear viscoelastic response and light scattering. Green and blue diamonds indicate, respectively, the theoretically estimated demixing and (MCT) liquid-glass lines in Fig. 5(b). Green filled circles at the left correspond to the low-ρ_S branch of the binodal calculated in the reservoir representation, as explained in Sec. 4.1 and Fig. 13; this branch is the same as the one of the system representation for $\rho_S \rightarrow 0$. The dashed line is a guide to the eye.

3.3.3 Rheological state diagram

The results from rheological measurements for systems characterized by $f = 214$ and $q = 3$ can be summarized through the experimental state diagram depicted in Fig. 9 for different combinations of star and hard sphere volume fractions. Data points above the glass line ($\rho_S \sigma_S^3 \gtrsim 0.327$) reflect discrete rheological measurements, based on which we identify the measured sample as liquid or solid, the latter being repulsive glass, arrested phase separation or double glass. Due to the limited amount of sample, this complete sequence of states is shown only for one value of star density ($\rho_S \sigma_S^3 = 0.343$). Below the glass line, i.e., $\rho_S < \rho_S^{(g)}$, no solid-like state was detected within the range of HS concentrations investigated. In that case, we experimentally assigned a transition to phase separation (demixing) by using DLS as is discussed in Section 4.2. The state diagram of Fig. 9 is the direct experimental counterpart of the theoretical diagram shown in Fig. 5(b), complementing the elastic modulus results of Fig. 8. Although the theory slightly overestimates the extent of the liquid state basin, as already pointed out in our previous work,[36] the experimental diagram fully confirms, in a quantitative and parameter-free fashion, the theoretical predictions showing liquid and (repulsive) glassy states, glass melting, demixing and a reentrant, solid-like state, which is linked to arrested phase separation.

Figure 10 shows the intensity autocorrelation functions for two different states measured by MSDLS at $\rho_S \sigma_S^3 = 0.343$ and colloid densities $\rho_H \sigma_S^3 = 0.024$ and $\rho_H \sigma_S^3 = 2.363$, respectively. The data show a slightly tilted plateau up to $t \geq 1$ s, at least four orders of magnitude larger than the relaxation time for diluted samples, which height is related to the non-ergodicity factor discussed in Section 3.2. At even larger times, a full decay of $G(Q,t)$ is ob-
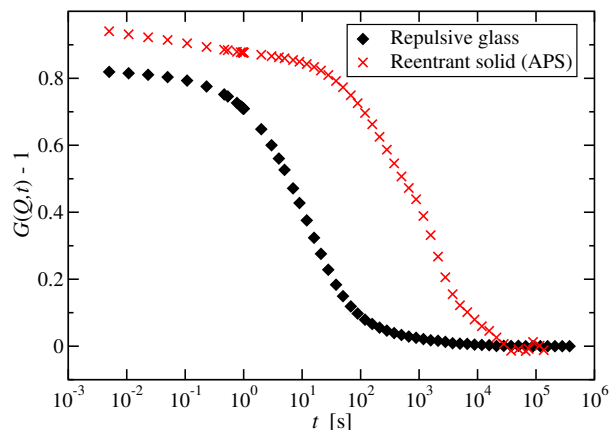
Fig. 10 MSDLS intensity auto-correlation function measured for $f = 214$, $q = 3$, $Q\sigma_S \simeq 1$, $\rho_S \sigma_S^3 = 0.343$ and two colloid concentrations $\rho_H \sigma_S^3 = 0.024$ (filled diamonds) and $\rho_H \sigma_S^3 = 2.363$ (crosses). The states of the two samples are attributed, respectively, to a repulsive glass and to a reentrant solid-like state, the latter being linked to arrested phase separation.

served, due to relaxation mechanisms not accounted for by the MCT calculations. This corroborates the suggested picture on two distinct glassy states, namely the usual, repulsive star glass and the solid state at the region of arrested phase separation. A quantitative comparison of the non-ergodicity factors requires separating the self- from collective contributions to the experimental non-ergodicity factor, which is a non-trivial task and will be the subject of future efforts.

4 Phase Separation

One of the main findings in the preceding section was the propensity of the system to demix upon addition of a sufficiently large number of colloidal particles. In what follows, we analyze quantitatively and rationalize theoretically this phenomenon by resorting to an effective one-component depletion picture, in which the colloids are canonically traced out, resulting in modified star-star interactions. This picture offers a transparent physical interpretation of the phenomenon and allows a straightforward and accurate calculation of the phase diagram in the mean-field approximation. Moreover, we present experimental evidence for the occurrence of this phase separation.

4.1 Theoretical approach

A useful and transparent way to gain insight into the effects of adding small, hard colloids to a high density star-polymer solution is to carry out a further coarse-graining procedure. In such a case, the mixture may be effectively considered as a one-component system, in which the stars interact not through the potential $V_{SS}(r)$ (see Eq. (4)) but rather through a colloid-modified effective potential $V_{SS}^{(mod)}(r)$, for which the degrees of freedom of the hard particles have been traced out. Formally, the colloid-modified, effective star-star interaction can be determined in the limit of vanishing ρ_S as

$$\beta V_{SS}^{(mod)}(r; \rho_H) = -\ln\left[g_{SS}(r; f, q, \rho_S \rightarrow 0, \rho_H)\right], \quad (15)$$

where the pair correlation function $g_{SS}(r)$ can be evaluated by solving the OZ-RY iteration, Eqs. (8)-(9), for the two-component mixture. By construction, this colloid-modified interaction potential leaves the correlation functions $g_{SS}(r)$ and $S_{SS}(k)$ between the stars invariant.[50,61] Writing $V_{SS}^{(\mathrm{mod})}(r)$ as the sum of the bare star-star interaction potential without any colloidal additive, plus a potential induced by the additive, a depletion-like contribution can be evaluated as

$$V_{\mathrm{dep}}(r;\rho_H) = V_{SS}^{(\mathrm{mod})}(r;\rho_H) - V_{SS}(r). \tag{16}$$

Figures 11 and 12 show representative results for the colloid-modified, effective star-star interaction and for the depletion interaction for different values of f, q and ρ_H. The depletion effect is stronger for increasing colloid densities, for larger colloid sizes (i.e., decreasing q), and increasing functionality of the stars. As ρ_H increases, the location of the $V_{SS}^{(\mathrm{mod})}$ minimum tends to $r \simeq 1.5\sigma_S \simeq 2R_S^{(g)}$. For shorter distances, the repulsive contribution coming from the overlap of the outer Daoud-Cotton blobs of the stars[42] rapidly counteracts the effect of the excess osmotic pressure due to the colloids, and dominates the effective interaction. Upon addition of the colloids, we thus have first a reduction in the repulsive interaction, leading to glass melting and subsequently, at higher colloid concentrations, to the development of effective, depletion-induced attractions between the stars that bring about the demixing, binodal line. The glass- and binodal lines meet, leading to the arrested phase separation.[10,39,40] Decreasing the size ratio q from 4 to 3 leads to a roughly two-fold increase in the depletion potential strength for the same ρ_H. As can be noted, all the depletion potential curves approach zero monotonically as the star-star distance increases, which contrasts with the case of binary hard-sphere mixtures, for which the development of oscillations in V_{dep} has been reported.[61,62] The same quantitative features are found also by employing the superposition approximation[35] to evaluate $V_{\mathrm{dep}}(r)$ (results not shown).

For systems with finite ρ_S, Eq. (15) can still be employed to map the binary mixture onto an effective one-component system. However in this case the potential should be determined at fixed chemical potential μ_C of the colloidal additive,[61] meaning that the colloid density in the system, ρ_H, has to be replaced by the colloid density of a reservoir ρ_H^r, which is such that μ_C in the reservoir and in the system coincide. In this way, the effective one-component description allows the determination of the phase behavior of the binary mixture in contact with a colloid reservoir, i.e., the calculation of the binodal line in the (ρ_S, ρ_H^r) plane. In the limit of low star density ($\rho_S \to 0$) the binodal calculated within this reservoir representation is identical to the one evaluated in the system representation, a fact that we have taken advantage of in Fig. 9. In what follows we work in this semigrand ensemble in which the density of stars ρ_S and the chemical potential of colloids μ_C are fixed, quoting the reservoir colloidal density ρ_H^r as an equivalent way of fixing the former.

On the basis of the two contributions to the full star-star potential, Eq. (16), we consider the pure star solution as a reference system and the colloid-induced star-star interaction $V_{\mathrm{dep}}(r)$ as a perturbation to it. Accordingly, a first-order $\lambda-$expansion can be
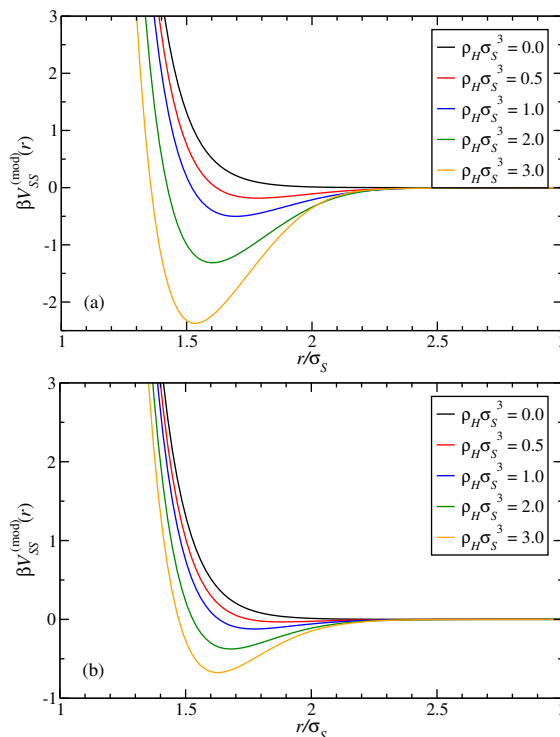
Fig. 11 Effective star-star interaction in the presence of colloids for $f = 300$. The colloid densities are indicated in the legends and the results are shown for two different size ratios: (a) $q = 3$; (b) $q = 4$.

performed to estimate the Helmholtz free energy per volume $\hat{f}(\rho)$ of the effective one-component system as

$$\begin{aligned} \hat{f}(\rho_S) &= \hat{f}_{\mathrm{ref}}(\rho_S) + \hat{f}_{\mathrm{dep}}(\rho_S, \rho_H^r) \\ &= \hat{f}_{\mathrm{id}}(\rho_S) + \hat{f}_{\mathrm{exc}}(\rho_S) + \hat{f}_{\mathrm{dep}}(\rho_S, \rho_H^r). \end{aligned} \tag{17}$$

The ideal contribution for the reference system is analytically known:

$$\hat{f}_{\mathrm{id}}(\rho_S) = k_B T \rho_S \left[\ln(\rho_S \sigma_S^3) - 1 + 3\ln(\Lambda_S/\sigma_S) \right], \tag{18}$$

where the last term, involving the thermal de Broglie wavelength Λ_S of the stars, is irrelevant and can be dropped. The excess part of the reference system can be obtained by using the thermodynamic relationship $P = -(\partial F/\partial V)_{N,T}$ connecting the pressure P to the Helmholtz free energy F and applied to their excess part:
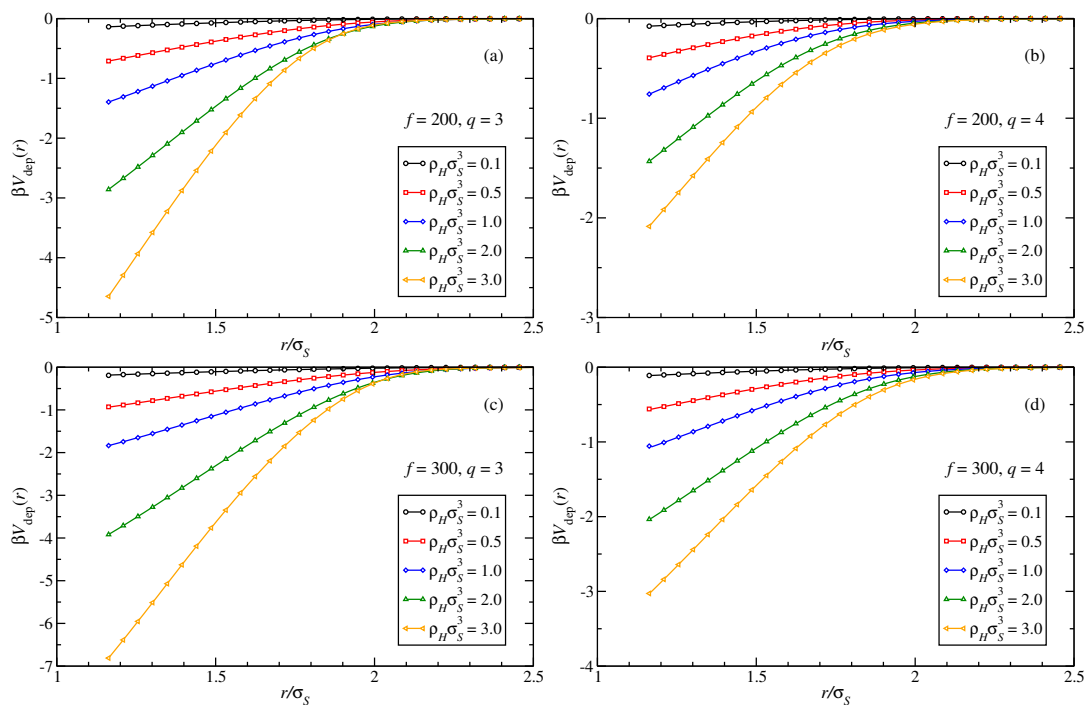
$$\hat{f}_{\mathrm{exc}}(\rho_S) = \rho_S \int_0^{\rho_S} d\rho \, \frac{P_{\mathrm{exc}}(\rho)}{\rho^2}, \tag{19}$$

the integrand being expressed as:[50]

$$\frac{P_{\mathrm{exc}}(\rho)}{\rho^2} = -\frac{2\pi}{3} \int_0^\infty dr \, r^3 \, V_{SS}'(r) \, g_{SS}^{(\mathrm{ref})}(r;\rho). \tag{20}$$

Finally, the mean-field approximation for the contribution of the attractive depletion potential to the free energy reads as:

$$\frac{\hat{f}_{\mathrm{dep}}(\rho_S, \rho_H^r)}{2\pi\rho_S} = \rho_S \int_0^\infty dr \, r^2 \, V_{\mathrm{dep}}(r, \rho_H^r) \, g_{SS}^{(\mathrm{ref})}(r, \rho_S). \tag{21}$$

Fig. 12 Depletion interactions induced on stars of functionality f by colloids at density $\rho_H \sigma_S^3$ and size ratios q as indicated at the legends.

In Eqs. (20)-(21), $g_{SS}^{(ref)}(r, \rho_S)$ and $V'_{SS}(r)$ are, respectively, the pair correlation function of the reference system and the derivative of the potential, and $V_{dep}(r, \rho_H^r)$ is determined by Eq. (16).

The mean-field calculation of $f(\rho_S)$ performed provides a direct method to track the convexity change of the free energy curve at high enough (reservoir) colloidal density, which leads to phase separation (demixing). In this way, the binodal line can be determined in the (ρ_S, ρ_H^r) representation by employing the common-tangent construction, which allow to account for the partial densities of both coexisting phases. Figure 13 displays the binodal lines for different values of f and q. In agreement with estimates based on the non-additivity parameter,[41] phase separation is observed at higher colloid reservoir densities for smaller colloid particles, as well as for softer stars. In the case $q = 8$, no phase separation was found probably because the necessary colloid density is much higher than the range considered. For the experimental system $f = 214$ and $q = 3$, we employed the modified effective potential $V_{SS}^{(mod)}(r; \rho_H^r)$ as input to theoretically evaluate both $S(Q)$ and $\phi(Q)$. The resulting (MCT) liquid-glass line crosses the binodal driving the phase separation to an arrested state, as plotted in Fig. 13. This scenario is reminiscent of the one found in hard spheres suspensions with long- and intemediate-range attractive interactions, which phase diagram is sketched in Fig. 13(b).[37,38] A similar behavior is expected for larger functionalities and size ratios with the glass line shifted to lower star density. Note that these trends are in complete agreement with the predictions made in the state diagrams (Figs. 5 and 6) based on the convergence limit of the OZ-RY approach to study the structure of the mixture, and also with the assumption of an arrested phase separation above this convergence line. In this way, the generic behavior of the mixture can be schematically represented as in Fig. 13(a).

## 4.2 Experimental evidence for phase separation

One of the experimental challenges is the detection of the arrested phase separation predicted by the theoretical analysis. From the experimental standpoint, it is advantageous for this purpose to explore phase separation in mixtures below the glass transition. Maintaining the star volume fraction constant while increasing
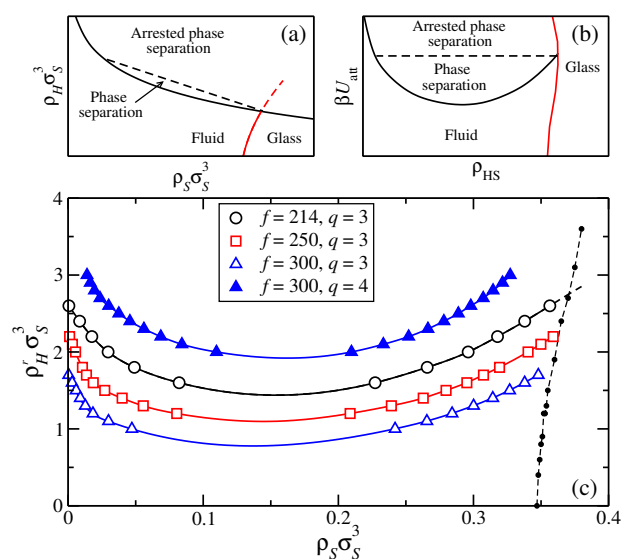
Fig. 13 Top: Schematic phase diagram for star-colloid mixtures in the system representation [(a)] and for hard-sphere systems with long-range attractive interaction[37,38] [(b)]. Bottom, (c): Demixing binodal lines in the reservoir representation for different functionalities and size ratios, as indicated in the legend. Small filled circles indicate the MCT liquid-glass line calculated using the modified, effective potential $V_{SS}^{(mod)}(r; \rho_H^r)$ for $f = 214$ and $q = 3$.
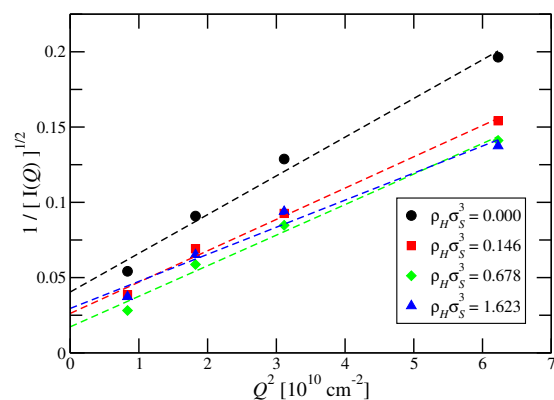
Fig. 14 Inverse square root of the average scattering intensity $1/\sqrt{I(Q)}$ vs. Q^2 for $\rho_S\sigma_S^3 = 0.126$ and different hard colloid densities. Dashed lines represent linear fits according to the Debye-Bueche model (Eq. (22)).
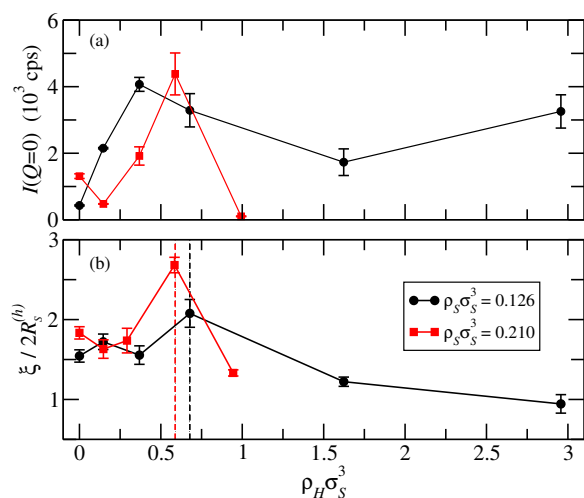

Fig. 15 (a) Average scattering intensity at $Q = 0$ and (b) correlation length normalized to the nominal (hydrodynamic) diameter of the star for $f = 214$, $q = 3$ and two different star concentrations as function of colloid density. The vertical dashed lines identifies the colloid density at which ξ attains the maximum value, which identifies the phase separation.

concentration of hard colloids, we have examined phase separation via dynamic/static light scattering by measuring the average scattering intensity at different wavevector Q, as shown in the Fig. 14. As the phase separation boundary is approached, the correlation length of the density fluctuations grows and lastly diverges. Concomitantly, it is expected that the measured scattering intensity at $Q \to 0$ will be a non-monotonic function of the parameter controlling the transition and attain a peak around the transition point. To evaluate both the correlation length ξ and the intensity $I(0)$, we made use of the Debye-Bueche analysis, which is appropriate for circularly symmetric scattering elements. For this model the scattering intensity $I(Q)$ can be described by the scattering function:[46]

$$I(Q) = \frac{I(0)}{\left[1 + (\xi Q)^2\right]^2}. \quad (22)$$

Figure 15 diplays the intensity at $Q = 0$ and the correlation length ξ determined from the total scattering intensity as function
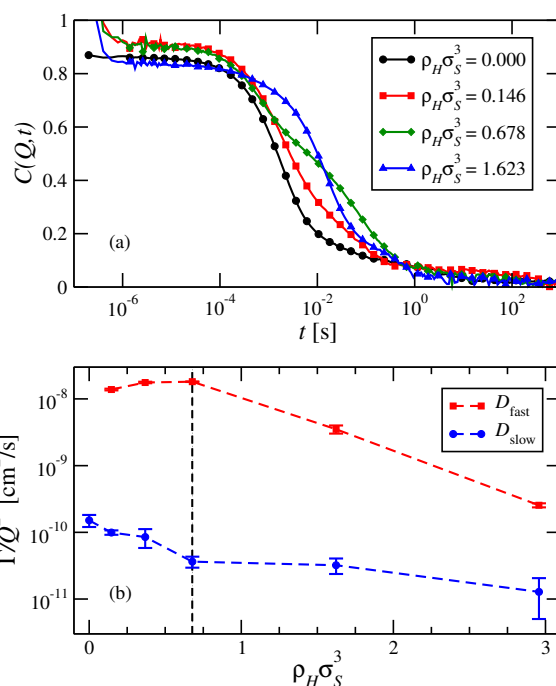
Fig. 16 (a) Typical DLS intermediate scattering functions for $\phi_S = 0.6$ $(\rho_S\sigma_S^3 = 0.126)$ at scattering angle $\theta = 30°$ $(Q\sigma_S = 1.12)$ and at increasing colloidal concentrations. Note that for $\rho_H > 0$ two relaxation processes are detected, while for $\rho_C = 0$ only one is observed. (b) The apparent diffusion coefficient at $\phi_S = 0.6$ $(\rho_S\sigma_S^3 = 0.126)$ as function of colloid density. Diffusion of the fast and slow processes are attributed to hard and soft colloids, respectively. The vertical dashed line is the same as in Fig. 15, splitting the diagram in the homogeneous and the phase separated regions.

of the hard sphere concentration by linear fitting $1/\sqrt{I(Q)}$ vs. Q^2 according to Eq. (22). The data correspond to two effective volume fractions of stars $\phi_S = c_S/c_S^* = 0.6$ and 1.0 ($\rho_S\sigma_S^3 = 0.126$ and 0.210, respectively) and indicate that with the addition of hard spheres, the star correlation length increases, which is also accompanied with an increase of the scattering intensity far below from the first peak of the structure factor ($Q \ll Q_{peak}$), thus conforming to an incipient phase separation. Here the transition region for $\phi_S = 1.0$ is also characterized by a (weak) increase in turbidity, in addition to the increase of ξ. At higher colloid fractions beyond the binodal line a correlation length is still measurable (the sample is turbid albeit not substantially) and it is indeed expected to decrease with increasing colloid fraction. As the schematic, theoretical phase diagram in Fig. 13 suggests, for higher ρ_S demixing occurs at lower ρ_H and therefore, at fixed colloid concentration, the correlation length should be shorter for $\phi_S = 0.6$ than for $\phi_S = 1.0$, which is in agreement with the experimental findings. Although the limited range of Q values considered in DLS gives rise to uncertainty in the estimation of the correlation length, the results are unambiguous for the purpose of the present study, i.e., they confirm the presence of phase separation through the non-monotonic behavior of the $\xi(\rho_H)$.

Further analysis of the DLS data provides additional evidence for phase separation. Typical intermediate scattering functions $C(Q,t)$ at $Q\sigma_S = 1.12$ for $\rho_S\sigma_S^3 = 0.126$ and various hard sphere

concentrations are depicted in the Fig. 16(a). Two (fast and slow) relaxation processes can be observed for $\rho_H > 0$, which relaxation rates Γ are plotted in Fig. 16(b) in the form of an apparent diffusion coefficient $D = \Gamma/Q^2$. The fast process is attributed to the hard spheres since at low colloid fractions, the extracted diffusion coefficient yields the hydrodynamic radius of the hard-like particles from the Stokes-Einstein-Sutherland equation. Up to the hard colloid density at which ξ is maximum ($\rho_H \sigma_S^3 = 0.678$, see Fig. 15), this diffusion coefficient is practically independent of colloid concentration. It then slows down rather dramatically in the phase separated region. At the same time, the diffusion coefficient of the slow mode, which is attributed to star-related motions, slows down for increasing colloid fractions (see Fig. 16). However the slow-down is sharper in the pre-transitional homogeneous region, conforming to the respective increase in correlation length.

5 Discussion

The results obtained show the strong influence of the size ratio q on the properties of star polymer and colloid binary mixtures. While for very small colloidal additive ($q \gtrsim 8$) the glassy behavior of dense star polymer suspensions remains unaffected, mid-sized colloid particles weaken the repulsion between the stars and provoke melting of the glass. Colloidal particles that are even larger ($q \lesssim 4$) tend to force the system into phase separation, as can be seen in Figs. 5 and 6. Although the binodal line was not evaluated, the convergence line presented in some of these state diagrams is a first approximation providing a good estimate for demixing of the binary mixtures. When the functionality f of the star is considered, the same generic trends are observed and as f decreases, a higher concentration of colloidal particles can be added before either melting of the glass or demixing occurs. This effect can be explained by the softness of the stars and the ability for small additives to penetrate them more easily. Softer star polymers therefore form more stable mixtures, which can be tuned by adjusting the amount and the size ratio of the colloidal additive, leading to glass softening and melting.

The results of the coarse-grained model employed were supported by the experimental findings from DLS and rheology in the particular case of $f = 214$ and $q = 3$ (Figs. 9 and 16). However it is important to note that this model assumes a much smaller size for the monomers (or more strictly the Kuhn length) forming the star arms as compared to the colloid size. Therefore it is to be expected that for high enough colloid densities, real mixtures will always phase separate as a consequence of the finite excluded volume between the Kuhn segments and the colloids, in a manner similar to the one found by MC simulations in the low functionality case ($f < 30$).[13,63]

The physical mechanism bringing about melting of the glassy state and the subsequent demixing transition can be attributed to the fact that the small colloids act like depletants for the large stars. From the point of view of effective interactions, the colloid-induced depletion is superimposed on the soft repulsion between stars, as shown in Fig. 11 for the low star density limit. A moderate colloid additive concentration causes the reduction in the star-star repulsion, leading to melting of the glass.[20,23] Upon fur-

ther increase in ρ_H, the net attractive potential between the stars rises, which drives the phase separation, as corroborated by rheology measurements at high ρ_S (Fig. 8). The depletion interaction seems to behave linearly at small distances r and becomes more attractive for larger functionalities and for larger (reservoir) densities of colloidal additives. Although the range of the attractive contribution shrinks by a few percent ($< 3\%$) as more colloids are added, it depends very weakly on the size ratio (Fig. 12). On the contrary, an increase in the latter leads to a markedly weaker depletion effect and therefore to a well-mixed system, while for similar sizes of polymer stars and colloids, the system demixes even for small amounts of additive.

The previously described behavior can be more clearly represented in a simplified picture allowing a full mapping of the two-component star polymer - colloid mixture to an effective one-component description. By employing the colloid-modified, star-star effective potential, a perturbation approach clearly showed that the binodal lines come down to small colloidal reservoir densities, as either the size ratio q is decreased or the functionality f is increased (Fig. 13). It is worth noting that for a system having a high enough ρ_H, the demixing could be arrested in the sense that ρ_S in the star-rich phase would lie beyond the liquid-glass line ($\rho_S \sigma_S^3 \sim 0.35$ for the considered f values) and, therefore this phase will be in a glassy state. The nature of the latter can be associated to a purely repulsive glass just above reentrance, as concluded by comparing its plateau modulus with that of the original glass, i.e., without colloids, as illustrated in Fig. 8. For colloidal densities well within the binodal, depletion attractions are stronger and can lead to arrest into an attractive glass characterized by a much higher modulus values.[36]

For dense suspensions of hard-spheres the addition of small, non-adsorbing polymers ($q < 0.1$) also leads to a reentrant glass transition. At sufficiently high densities, the pure colloidal system reaches a repulsive glassy state in which the dynamic arrest is a consequence of caging among the particles. Once a small amount of polymer is added, the induced depletion potential makes the particles cluster, loosening the cages and therefore restoring the ergodicity (i.e. melting the glass). A further increase in polymer concentration leads to a different kind of arrest due to long-lived bonds between the particles, giving rise to an attraction-dominated glass.[64] On the other hand for larger polymers, $q \simeq 0.6$, the situation is quite similar to that previously described in the system at hand. As the range of the attraction increases, the region of demixing increases in stability relatively to the glass-line, and therefore a range of compositions can be found for which the phase separation can take place without being arrested, as can be see in Fig. 13(b). However still deeper quenches could lead to kinetic arrest and even to gel formation.[65–67]

To contrast the systems considered with their hard counterpart, it is interesting to note that the size (and conformation) of the stars is not significantly perturbed by the addition of a small amount of hard depletants, because the star osmotic pressure is weakly increased. However as ρ_H approaches the hard sphere glass transition, $\rho_H \to \rho_H^{(g)}$, the osmotic pressure abruptly increases and leads to the virtual collapse of the soft stars with a concomitant jump in G_p, which reaches a slightly larger value of

the elastic modulus than the one for pure hard sphere-like glasses at the same ϕ_H (without soft stars added), as shown in Fig. 8. A further increase in G_p at higher colloid fractions is attributed to the reinforcing effect of the hard spheres, as the stars cannot further shrink and a double-glass of asymmetric hard spheres is formed. The transition to the double glass at a colloid volume fraction $\phi_H \gtrsim 0.75$ is promoted by the action of osmotic forces of colloids which reduced the size of the stars and the reduced available space and large concentrations of both components. The possible formation of an attractive glass also cannot be excluded, since the effective colloid-to-star size ratio is increased proportionally to the shrinkage factor (α_S) from $\zeta = 0.25$ $(q = 3)$ to $\zeta \simeq 0.72$ $(q \simeq 1)$, as shown in Fig. 8. On the other hand, this is an arrested phase separation regime, providing the driving force for star attraction (depletion). This cannot be currently further examined, so we leave it as a speculation worth investigating in the future.

6　Conclusions

We analyzed the impact that the addition of small, hard colloids $(q > 2)$ has on the behavior of suspensions of large star polymers with a high functionality $(f \gtrsim 200)$. While three and higher body effects are expected to play a significant role at high densities,[68] we were still able to demonstrate the adequacy of a recently introduced coarse-grained model, based on effective pair interactions, to predict the structure and the phase behavior of mixtures well above the overlapping density as function of their composition.[36,41] As the concentration of depletant is increased several rheological states are detected, including phase separation (demixing) of a fluid-like suspension (at low star densities) and the melting of a repulsive glassy state (at high star densities). We made use of DLS/SLS to detect phase separation in liquid-like samples and rheology to detect repulsive glass melting and reentrant solid-like states above the glass line of the colloid-free system. In the latter case, as the depletant concentration is further increased, interplay between structural arrest and demixing takes place, leading to an arrested phase separation and therefore to a new re-entrant glassy state, as shown in Figs. 5, 6, and 13. This theoretically predicted behavior was corroborated by experimental studies of the dynamics of stars via DLS as well as the linear viscoelastic response of the mixtures for different hard sphere concentrations; moreover, distinct signatures of the nature of the reentrant glass were identified.

In contrast to the classic colloid-polymer example, which exhibits attractive vitrification upon continuous addition of small depletants to the originally glassy suspension of hard colloids, here the behavior is much richer, as depicted in Fig. 9. As depletant is added to a suspension at fixed star density, soft repulsion and long-range attraction between the stars develop (see Figs. 11 and 12). Due to this depletion effect, the initial repulsive glass melts. However, as depletant is added beyond the demixing line, the increase in total concentration compensates for the reduced repulsion and a reentrant solid-like state is found.[36] This state has essentially the same plateau modulus G_p as the originally colloid-free suspension, i.e. the glassy state has a repulsive nature. At higher depletant concentrations, the stronger attractive contri-

bution leads to arrest into an attractive glass featuring a much higher modulus. At the same time, the soft nature of the stars begins to play a more important role since the presence of hard spheres induces star shrinkage, which is strongly correlated with the crossover found in the dependence of the plateau modulus on the colloid density, as can be seen in Fig. 8.

The results presented here complement previous considerations on mixtures of hard colloids and star polymers in the colloidal limit $(q < 1)$,[34] making it now possible to reliably describe the macroscopic behavior of such mixtures in the full range of size ratios q and star functionalities f. Moreover, these enrich to a large extent the findings for binary mixtures of star polymers. As stars with a smaller size and lower functionality $(q < 0.5, f < 64)$ are added to a glass of high functionality stars $(f > 250)$, multiple reentrant behaviors were described including single, double, and asymmetric glass regions, as well as an arrested phase separation region depending on the size asymmetry q and the concentration of the small component.[20,21] As reported by Zaccarelli *et al.*,[56] from a dynamic point of view this rich reentrant glass scenario has as prerequisite not only a large size asymmetry but also that the short-time mobility of the added component be much higher than that of the glass-forming species.

The system investigated is highly deformable and shares many features with different hyperbranched polymers including microgels, copolymer micelles, polymer-grafted nanoparticles and dendrimers, all of which can be well-described through a core-shell structure and whose interactions can be easily tuned through several physical and chemical factors. Since the theoretical description is independent of adjustable fitting parameters, we expect our results to hold for more generic systems, which offer interesting insight into the design and precise tunability of new soft composites that are of great interest in materials science and industrial applications.

Acknowledgements

References

1　R. Verma, J. C. Crocker, T. C. Lubensky and A. G. Yodh, *Phys. Rev. Lett.*, 1998, **81**, 4004–4007.

2　Y. N. Ohshima, H. Sakagami, K. Okumoto, A. Tokoyoda, T. Igarashi, K. B. Shintaku, S. Toride, H. Sekino, K. Kabuto and I. Nishio, *Phys. Rev. Lett.*, 1997, **78**, 3963–3966.

3　C. Bechinger, D. Rudhardt, P. Leiderer, R. Roth and S. Dietrich, *Phys. Rev. Lett.*, 1999, **83**, 3960–3963.

4   W. Poon, *Science*, 2004, **304**, 830–831.

5   S. Asakura and F. Oosawa, *J. Polym. Sci.*, 1958, **33**, 183–192.

6   A. Vrij, *Pure Appl. Chem.*, 1976, **48**, 471.

7   K. Dawson, G. Foffi, M. Fuchs, W. Götze, F. Sciortino, M. Sperl, P. Tartaglia, T. Voigtmann and E. Zaccarelli, *Phys. Rev. E*, 2000, **63**, 011401.

8   K. N. Pham, A. Puertas, J. Bergenholtz, S. U. Egelhaaf, A. Moussaïd, P. N. Pusey, A. B. Schofield, M. E. Cates, M. Fuchs and W. C. K. Poon, *Science*, 2002, **296**, 104–6.

9   A. M. Puertas, M. Fuchs and M. E. Cates, *J. Phys. Chem. B*, 2005, **109**, 6666–6675.

10 A. M. Puertas, M. Fuchs and M. E. Cates, *J. Phys.: Condens. Matter*, 2007, **19**, 205140.

11 P. G. Bolhuis, E. J. Meijer and A. A. Louis, *Phys. Rev. Lett.*, 2003, **90**, 14–17.

12 K. J. Mutch, J. S. van Duijneveldt and J. Eastoe, *Soft Matter*, 2007, **3**, 155.

13 N. A. Mahynski, T. Lafitte and A. Z. Panagiotopoulos, *Phys. Rev. E*, 2012, **85**, year.

14 C. N. Likos, *Soft Matter*, 2006, **2**, 478.

15 D. Vlassopoulos and G. Fytas, *High Solid Dispersion*, Springer Berlin Heidelberg, 2010, vol. 236, pp. 1–54.

16 C. N. Likos, H. Löwen, M. Watzlawek, B. Abbas, O. Jucknischke, J. Allgaier and D. Richter, *Phys. Rev. Lett.*, 1998, **80**, 4450–4453.

17 M. Watzlawek, C. N. Likos and H. Löwen, *Phys. Rev. Lett.*, 1999, **82**, 5289.

18 G. Foffi, F. Sciortino, P. Tartaglia, E. Zaccarelli, F. Lo Verso, L. Reatto, K. A. Dawson and C. N. Likos, *Phys. Rev. Lett.*, 2003, **90**, 238301.

19 E. Zaccarelli, C. Mayer, A. Asteriadi, C. N. Likos, F. Sciortino, J. Roovers, H. Iatrou, N. Hadjichristidis, P. Tartaglia, H. Löwen and D. Vlassopoulos, *Phys. Rev. Lett.*, 2005, **95**, 268301.

20 C. Mayer, E. Zaccarelli, E. Stiakakis, C. N. Likos, F. Scortino, A. Munam, M. Gauthier, N. Hadjichristidis, H. Iatrou, P. Tartaglia, H. Löwen and D. Vlassopoulos, *Nat. Mater.*, 2008, **7**, 780–784.

21 C. Mayer, F. Sciortino, C. N. Likos, P. Tartaglia, H. Löwen and E. Zaccarelli, *Macromolecules*, 2009, **42**, year.

22 E. Stiakakis, B. M. Erwin, D. Vlassopoulos, M. Cloitre, A. Munam, M. Gauthier, H. Iatrou and N. Hadjichristidis, *J. Phys.: Condens. Matter*, 2011, **23**, 234116.

23 E. Stiakakis, D. Vlassopoulos, C. N. Likos, J. Roovers and G. Meier, *Phys. Rev. Lett.*, 2002, **89**, 208302.

24 E. Stiakakis, G. Petekidis, D. Vlassopoulos, C. N. Likos, H. Iatrou, N. Hadjichristidis and J. Roovers, *Europhys. Lett.*, 2005, **72**, 664.

25 C. Mayer and C. N. Likos, *Macromolecules*, 2007, **40**, 1196–1206.

26 M. Camargo and C. N. Likos, *J. Chem. Phys.*, 2009, **130**, 204904.

27 B. Lonetti, M. Camargo, J. Stellbrink, C. N. Likos, E. Zaccarelli, L. Willner, P. Lindner and D. Richter, *Phys. Rev. Lett.*, 2011, **106**, 228301.

28 M. Camargo, S. A. Egorov and C. N. Likos, *Soft Matter*, 2012, **8**, 4177.

29 T. Wang and J. L. Keddie, *Adv. Colloid Interface Sci.*, 2009, **147-148**, 319–32.

30 S. K. Kumar and R. Krishnamoorti, *Ann. Rev. Chem. Biomol. Eng.*, 2010, **1**, 37.

31 H.-Y. Yu, S. Srivastava, L. A. Archer and D. L. Koch, *Soft Matter*, 2014, **10**, 9120–9135.

32 S. Choudhury, A. Agrawal, S. A. Kim and L. A. Archer, *Langmuir*, 2015, **31**, 3222–3231.

33 J. Dzubiella, A. Jusufi, C. N. Likos, C. von Ferber, H. Löwen, J. Stellbrink, J. Allgaier, D. Richter, A. Schofield, P. Smith, W. Poon and P. Pusey, *Phys. Rev. E*, 2001, **64**, 010401(R).

34 A. Jusufi, J. Dzubiella, C. N. Likos, C. von Ferber and H. Löwen, *J. Phys.: Condens. Matter*, 2001, **13**, 6177–6194.

35 J. Dzubiella, C. N. Likos and H. Löwen, *J. Chem. Phys.*, 2002, **116**, 9518.

36 D. Truzzolillo, D. Marzi, J. Marakis, B. Capone, M. Camargo, A. Munam, F. Moingeon, M. Gauthier, C. N. Likos and D. Vlassopoulos, *Phys. Rev. Lett.*, 2013, **111**, 208301.

37 G. Foffi, C. D. Michele, F. Sciortino and P. Tartaglia, *Phys. Rev. Lett.*, 2005, **94**, 078301.

38 F. Cardinaux, T. Gibaud, A. Stradner and P. Schurtenberger, *Phys. Rev. Lett.*, 2007, **99**, 118301.

39 V. Testard, L. Berthier and W. Kob, *Phys. Rev. Lett.*, 2011, **106**, 125702.

40 V. Testard, L. Berthier and W. Kob, *J. Chem. Phys.*, 2014, **140**, 164502.

41 D. Marzi, C. N. Likos and B. Capone, *J. Chem. Phys.*, 2012, **137**, 014902.

42 M. Daoud and J. P. Cotton, *J. Phys. (Paris)*, 1982, **43**, 531.

43 D. Truzzolillo, D. Vlassopoulos and M. Gauthier, *Macromolecules*, 2011, **44**, 5043–5052.

44 J. Roovers, L. L. Zhou, P. M. Toporowski, M. V. D. Zwan, H. Iatrou and N. Hadjichristidis, *Macromolecules*, 1993, **26**, 4324–4331.

45 M. Gauthier and A. Munam, *Macromolecules*, 2010, **43**, 3672–3681.

46 B. J. Berne and R. Pecora, *Dynamic Light Scattering*, Dover, New York, 2000.

47 S. W. Provencher, *Comput. Phys. Commun.*, 1982, **27**, 229.

48 A. Wong and P. Wiltzius, *Rev. Sci. Instrum.*, 1993, **64**, 2547.

49 S. Kirsch, V. Frenz, W. Schärtl, E. Bartsch and H. Sillescu, *J. Chem. Phys.*, 1996, **104**, 1758.

50 J. P. Hansen and I. McDonald, *Theory of Simple Liquids*, Academic Press, London, 2006.

51 J. Dzubiella, C. N. Likos and H. Löwen, *Europhys. Lett.*, 2002, **58**, 133–139.

52 B. Loppinet, E. Stiakakis, D. Vlassopoulos, G. Fytas and J. Roovers, *Macromolecules*, 2001, **34**, 8216.

53 E. Stiakakis, A. Wilk, J. Kohlbrecher, D. Vlassopoulos and G. Petekidis, *Phys. Rev. E*, 2010, **81**, 020402.

54 W. Götze, *Liquids Freezing and the Glass Transition: Les*

Houches Session LI, North-Holland, Amsterdam, 1991.

55 E. Zaccarelli, *Physics of Complex Colloids*, IOS Press, 2013, pp. 95–154.

56 E. Zaccarelli, H. Löwen, P. P. F. Wessels, F. Sciortino, P. Tartaglia and C. N. Likos, *Phys. Rev. Lett.*, 2004, **92**, 225703.

57 K. N. Pham, G. Petekidis, D. Vlassopoulos, S. Egelhaaf, W. Poon and P. Pusey, *J. Rheol.*, 2008, **52**, 649.

58 C. Likos, H. Löwen, A. Poppe, L. Willner, J. Roovers, B. Cubitt and D. Richter, *Physical Review E*, 1998, **58**, 6299.

59 M. A. Rutgers, J. H. Dunsmuir, J. Z. Xue, W. B. Russel and P. M. Chaikin, *Phys. Rev. B*, 1996, **53**, 5043.

60 T. Voigtmann, *Europhys. Lett.*, 2011, **96**, 36006.

61 M. Dijkstra, R. van Roij and R. Evans, *Phys. Rev. Lett.*, 1999, **82**, 117–120.

62 R. Roth, R. Evans and S. Dietrich, *Phys. Rev. E*, 2000, **62**, 5360–5377.

63 N. A. Mahynski and A. Z. Panagiotopoulos, *J. Chem. Phys.*, 2013, **139**, 024907.

64 K. N. Pham, S. U. Egelhaaf, P. N. Pusey and W. Poon, *Phys. Rev. E*, 2004, **69**, 011503.

65 G. Foffi, K. A. Dawson, S. V. Buldyrev, F. Sciortino, E. Zaccarelli and P. Tartaglia, *Phys. Rev. E*, 2002, **65**, 050802.

66 L. J. Teece, M. A. Faers and P. Bartlett, *Soft Matter*, 2011, **7**, 1341.

67 I. Zhang, C. P. Royall, M. A. Faers and P. Bartlett, *Soft Matter*, 2013, **9**, 2076.

68 C. von Ferber, A. Jusufi, C. N. Likos, H. Löwen and M. Watzlawek, *Eur. Phys. J. E*, 2000, **2**, 311.
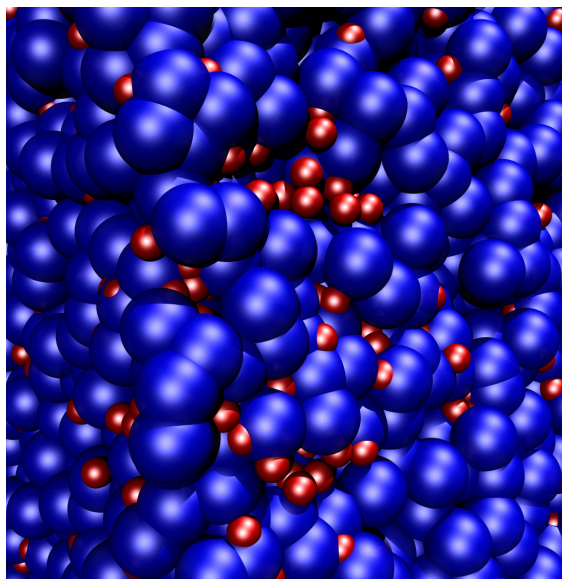
Graphical abstract: Coarse-grained representation of a binary mixture of large star-polymers (blue) and small hard colloids (red).